MICELLE FORMATION THERMODYNAMICS AND THE ACOUSTIC AND RHEOLOGICAL PROPERTIES OF AQUEOUS SODIUM p–n OCTYLBENZENESULFONATE SOLUTIONS

M. K. Karabaev, A. A. Saidov,
A. P. Voleishis, L. V. Pal'chikova,
and P. K. Khabibullaev

UDC 539.1:534.286

It is shown that the speed of sound and the adiabatic compressibility give a reasonably full characterization of the processes occurring in a surfactant + water system, including the phase transition on micelle formation.

The molecules of a surfactant (SA) are amphiphilic, i.e., the hydrophilic polar or ionic group in the molecule is accompanied by a hydrophobic radical. The dissolution of an ionogenic SA is accompanied by interaction between the charged group and the water molecules.

Above a certain size for the hydrophobic radical, the dissolved ions associate in a microheterogeneous micella structure. Micelles are formed in a comparatively narrow concentration range C_c, which is called the critical micelle concentration (CMC), and the micelles are in dynamic equilibrium with the amphiphilic ions. Although there have been many studies on micelle formation [1], the nature of it has not been finally elucidated.

For this reason, new evidence on the parameters of SA solutions in that range is important in establishing the nature of the process and in defining effective ways of controlling the properties of micella systems and accelerating their practical use.

As micelles are formed in very dilute solution and over a narrow concentration range, at least for ionogenic SA, while the specific physicochemical parameters show only slight changes, there are certain difficulties in making measurements near the CMC. Therefore, studies such as [2] amount mainly to indirect determination of the CMC, establishing the structure of the existing micelles above the critical concentration, qualitative process description, and thermodynamic-characteristic evaluation.

We have examined the rheological and acoustic parameters of SA solutions, which have a bearing on the spontaneous molecular association. We used aqueous solutions of sodium p–n octylbenzenesulfonate (OBS).

We measured the effects of OBS concentration at 293-313°K on the density ρ, viscosity η, and speed of sound u. The density was determined by hydrostatic weighing over the concentration range 2-20 mole/m^3 with an accuracy of ±0.005%.

The measurements on ρ showed that the density increases linearly with OBS concentration at a constant temperature, with a kink at the CMC. The behavior before and after the CMC is linear and is satisfactorily represented by

$$\rho = a + bc. \tag{1}$$

To describe experiments at concentrations higher than the GMC, instead of the concentration C one should use the value $C - C_c$. Table 1 gives the values of a, b, and C_c. As the temperature increases, the coefficients in (1) decrease at concentrations on both sides of the CMC, while the difference between them increases. Table 1 also gives the partial molar volumes of the OBS in the molecularly dispersed state V_2^s and in the micella state V_2^m; the difference ΔV_m^0 is given by

$$V_2^{s,m} = \frac{M}{\rho_{0,c}}\left[1 - \left(\frac{d\rho}{dC}\right)^{s,m}\right], \quad \Delta V_m^0 = V_2^s - V_2^m. \tag{2}$$

Thermophysics Division, Academy of Sciences of the Uzebek SSR, Tashkent. Translated from Inzhenerno-Fizicheskii Zhurnal, Vol. 50, No. 1, pp. 76-84, January, 1986. Original article submitted December 10, 1984.

0022-0841/86/5001-0063$12.50

TABLE 1. Parameters in (1) and (2)

T, K	C_c, mole/m^3	a, kg/m^3		b, kg/mole		$V_2^s \cdot 10^6$	$V_2^m \cdot 10^6$	$\Delta V_m^0 \cdot 10^5$
		below CMC	above CMC	below CMC	above CMC	m^3/mole		
293	10,0	998,15	998,85	0,070	0,052	222,8	240,6	17,8
303	11,0	995,60	996,37	0,070	0,047	223,4	246,5	23,1
313	12,0	992,15	992,98	0,069	0,040	225,1	254,1	29,0
323	13,0	987,98	988,79	0,062	0,030	233,3	265,5	32,2
333	15,0	983,18	984,05	0,058	0,020	238,6	276,9	38,3

TABLE 2. Parameters in (3), (4), and (5)

T, K	C_c^*, mole/m^3	$m \cdot 10^3$, Pa·sec	$K \cdot 10^3$, mole^{-1}·m^3·Pa·sec	$\eta_{CMC} \times 10^3$, Pa·sec	$[\eta] \cdot 10^3$, m^3/kg	δ, kg H_2O/kg OBS	h', mole H_2O/mole OBS
293	10,0	1,002	0,0025	1,002	8,6	2,61	42
303	11,0	0,798	0,0024	0,799	8,3	2,47	40
313	12,0	0,654	0,0015	0,654	7,9	2,27	37
323	13,0	0,549	0,0014	0,549	7,7	2,15	35
333	15,0	0,473	0,0010	0,473	7,3	1,94	31

Equation (2) can be used if the partial molar volume of the solute V_2 is independent of concentration. At the same time, V_2^s and V_2^m increase with temperature at different rates.

The viscosity of an OBS solution in the concentration range 2-20 mole/m^3 at 293-333°K was measured with a capillary viscometer with an accuracy of ±0.1%.

The viscosity measurements show that there is no change with the OBS concentration below the CMC at constant temperature within the error limits, whereas there is an increase above the CMC. The kink on the viscosity–concentration relation occurs at the CMC. An exception is represented by the viscosity at 60°C, where there is also some increase in viscosity below the CMC. In all the temperature ranges used, the viscosity is satisfactorily described by the following equation above the CMC:

$$\eta = K(C - C_c) + m. \tag{3}$$

Table 2 gives the coefficients in (3), together with C_c, the viscosity at the CMC η_{CMC}, and the characteristic viscosity $[\eta]$, which is derived from the empirical relation

$$[\eta] = \lim_{(C-C_c)\to 0} \frac{1}{C - C_c} \ln \frac{\eta}{\eta_{CMC}}. \tag{4}$$

The hydration δ_1 in kg H_2O/kg OBS was calculated from

$$\delta_1 = \frac{[\eta] - \nu\bar{v}_2}{\nu v_1^0}, \tag{5}$$

where ν is the Simha–Einstein form factor, which is 2.5 for a sphere. Table 2 gives h', which is the number of bound water molecules per OBS molecule in the micella state. Therefore, the density and viscosity far from the CMC are satisfactorily described by linear equations with differing coefficients in the temperature and concentration ranges used.

Speed of Sound. OBS solutions of concentration 2-16 mole/m^3 were used at 293°K to measure the speed of sound u by a resonance method at 2 MHz with double-distilled water, resolution ±0.1 m/sec. Figure 1 shows the results together with the adiabatic compressibility β_S calculated from $\beta_S = 1/\rho u^2$ if the speed of sound in double-distilled water at 293°K is taken as 1482.20 m/sec. We calculated β_S with the ρ defined by (1). It is evident from Fig. 1 that u and β_2 show discontinuities at a concentration of about 10 mole/m^3, while the behavior outside this region is close to linear. The linear parts of the C dependence of β_S are closely described by

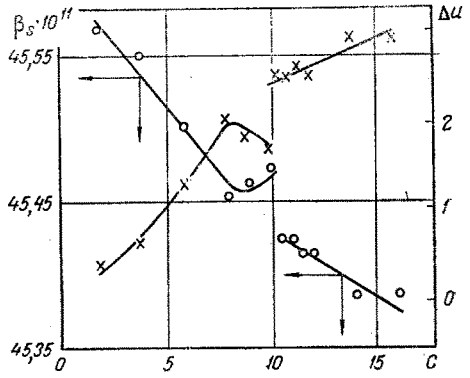

Fig. 1. Dependence of u and β_S on OBS concentration C at T = 293°K and f = 2 MHz.

TABLE 3. Dependence of the Measure Speed of Sound u on the Reduced Concentration ε at T = 293°K and f = 10.99838 MHz

ε	u, m/sec	ε	u, m/sec	ε	u, m/sec
0,2016	1484,09	0,0034	1484,60	0,0062	1484,65
0,1673	1484,17	0,0028	1484,60	0,0088	1484,66
0,1330	1484,27	0,0011	1484,60	0,0123	1484,67
0,0988	1484,34	0,0007	1484,60	0,0157	1484,68
0,0645	1484,46	0,0007	1484,58	0,0208	1484,69
0,0302	1484,53	0,0009	1484,60	0,0277	1484,70
0,0223	1484,56	0,0015	1484,61	0,0346	1484,71
0,0171	1484,58	0,0022	1484,62	0,0435	1484,72
0,0131	1484,59	0,0026	1484,63	0,0504	1484,75
0,0086	1484,60	0,0033	1484,64	0,0636	1484,77
0,0062	1484,60	0,0041	1484,65	0,0967	1484,86

$$\beta_s \cdot 10^{11} = (45.62 - 0{,}02C), \ \text{m} \cdot \text{sec}^2/\text{kg} \tag{6}$$

at concentrations less than the CMC and by

$$\beta_s \cdot 10^{11} = 45.43 - 0.0108\,(C - C_c), \ \text{m} \cdot \text{sec}^2/\text{kg} \tag{7}$$

above the CMC, C_c = 10 mole/m^3.

The speeds of sound measured with an accuracy of 0.1 m/sec do not enable one to determine the behavior of the adiabatic compressibility near the CMC. We therefore made precise measurements in the concentration range 8.0-11.0 mole/m^3 at 293°K with the frequency f = 10.99839 MHz by means of an interferometric method [3] with a resolution of ±0.01 m/sec. Table 3 gives the results, where the concentration is expressed in terms of ε, a dimensionless variable: $\varepsilon = (C - C_c)/C_c$ (C_c = 9.9590 mole/m^3 or 0.18012 × 10^{-3} molar parts).

Figure 2 shows the dependence of the speed of sound on ε throughout the range. There are three characteristic parts. In a wide region near the CMC, the speed of sound increases almost linearly with the total OBS concentration (parts I, concentrations above and below the CMC). As the CMC is approached from the left or right, there is a nonlinear variation (part II). Finally, directly at the CMC (ε < 0.01), there is a minimum in the speed of sound (part III). In part II on the true-solution side, the increase is somewhat more rapidly than linear, whereas in the same part on the micella side it is less so.

In the region of the minimum (part III), the picture alters radically. On the molecular-solution side, the speed remains approximately constant, whereas there is a steep change on the micella side.

The speed of sound is affected by the density and adiabatic compressibility, so to calculate β_S, we approximated the density by means of linear equations derived from hydrostatic measurements. In that case, the density is given by the following formulas derived from the coefficients of Table 1:

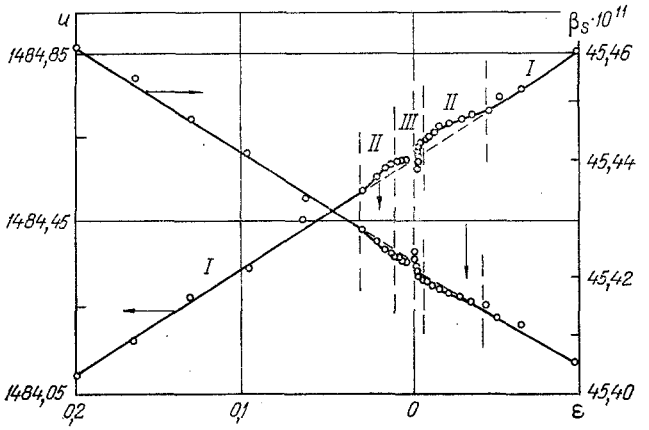

Fig. 2. Dependence of u and β_S on ε for T = 293°K and f = 10.99839 MHz.

TABLE 4. Effects of ε on the Values of ρ and β_S Calculated from (10) and (11)

ε	ρ, kg/m³	$\beta_s \cdot 10^{11}$, m·sec²/kg	ε	ρ, kg/m³	$\beta_s \cdot 10^{11}$, m·sec² /kg
0,2016	998,71	45,4611	0,0009	998,79	45,4263
0,1673	998,73	45,4553	0,0015	998,80	45,4252
0,1330	998,76	45,4478	0,0022	998,80	45,4246
0,0988	998,78	45,4426	0,0026	998,80	45,4240
0,0645	998,80	45,4344	0,0033	998,81	45,4229
0,0302*	998,83	45,4287	0,0041	998,81	45,4223
0,0223	998,81	45,4278	0,0062	998,82	45,4218
0,0171	998,80	45,4270	0,0088	998,83	45,4208
0,0131	998,79	45,4269	0,0123	998,83	45,4202
0,0086	998,78	45,4267	0,0157	998,84	45,4191
0,0062	998,77	45,4272	0,0208	998,85	45,4180
0,0034	998,76	45,4276	0,0277*	998,86	45,4170
0,0028	998,76	45,4276	0,0346	998,87	45,4159
0,0011	998,75	45,4281	0,0435	998,87	45,4153
0,0007	998,74	45,4285	0,0504	998,88	45,4130
0,0007	998,79	45,4275	0,0636	998,88	45,4118
			0,0967	998,90	45,4053

*Point of transition from the linear behavior of ρ to nonlinear or vice versa.

$$\rho = (998.85 - 0.7\varepsilon) \text{ kg/m}^3 \tag{8}$$

below the CMC and

$$\rho (998.85 + 0.52\varepsilon) \text{ kg/m}^3 \tag{9}$$

above the CMC.

The values of ρ were calculated with an accuracy of $\pm 5 \times 10^{-3}$ kg/m³. The concentration dependence (Fig. 2) shows that the adiabatic compressibility varies with the singularities found in the speed of sound, where the anomaly occurs at concentrations below and above the CMC.

The nonlinearity and reduction in the adiabatic compressibility are evidently due to incorrectness in the relations used to describe the density near the CMC.

In the second approximation with respect to concentration (indicated by arrows in Fig. 2), one can introduce a nonlinear term $\varepsilon^{1/2}$ into the density equation, which is usually employed to describe the density changes near critical points. It is necessary to impose an additional condition, namely that as many points as possible on the ε dependence of β_S should coincide with the linear behavior of the compressibility starting at certain concentrations. Calculations show that this condition is met by

$$\rho = 998.73 + 0.56\varepsilon^{1/2}, \text{ when } \varepsilon \leqslant 0.0302, \tag{10}$$

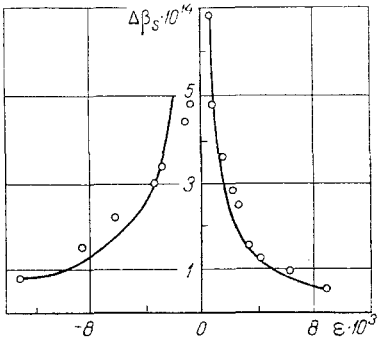

Fig. 3. Dependence of the singular part of the adiabatic compressibility $\Delta\beta_S$ on ε at T = 293°K and f = 10.99839 MHz.

below the CMC and

$$\rho = 998.73 + 0.48\varepsilon^{1/2}, \quad \text{when } \varepsilon \leqslant 0{,}0277, \tag{11}$$

above the CMC.

Table 4 gives the concentration dependence of the density derived from these equations. There is a constant difference at ρ_c of 0.05 kg/m^3, evidently because the reference linear relations are derived from experimental data where the error corridor was ±0.05 kg/m^3 and because there is a change in the partial molar volumes on transition through the CMC. Table 4 also gives values of β_S derived from the above approximation for the density. The data show that the compressibility varies linearly with the concentration as the CMC is approached but shows a divergence near the CMC. On extrapolating the linear parts of the ε dependence of β_S for $\varepsilon = 0$ obtained by approximation from opposite sides. Therefore, for correct description of β_S near the CMC, it is necessary to compare the $\Delta\beta_S$, namely the difference between the regular part and the observed curve near the divergence. The linear part may be represented by

$$\beta_s \cdot 10^{11} = (45.4237 + 0.186\varepsilon)\ \text{m}\cdot\text{sec}^2/\text{kg} \tag{12}$$

below the CMC and by

$$\beta_s \cdot 10^{11} = (45.4219 - 0.169\varepsilon)\ \text{m}\cdot\text{sec}^2/\text{kg} \tag{13}$$

above the CMC.

Figure 3 shows $\Delta\beta_S$ for various ε, as well as graphs for $\Delta\beta_S$ calculated from the following equations (curves):

$$\Delta\beta_s \cdot 10^{14} = (1 \cdot 10^{-2}\varepsilon^{-1})\ \text{m}\cdot\text{sec}^2/\text{kg} \tag{14}$$

below the CMC and

$$\Delta\beta_s \cdot 10^{14} = (0.5 \cdot 10^{-2}\varepsilon^{-1})\ \text{m}\cdot\text{sec}^2/\text{kg} \tag{15}$$

above the CMC.

The agreement is satisfactory apart from the two closest values of $\Delta\beta_S$ on the molecular-solution side. The preexponential coefficients are in the ratio 2:1.

It is therefore likely that the variation in u in the nonlinear parts II (Fig. 2) is associated mainly with the behavior of the density. The boundaries to the region where the adiabatic compressibility increases virtually coincide with those for the minimum in the speed of sound (part III in Fig. 2). One assumes that the density and the compressibility vary simultaneously as the OBS concentration varies in this region.

The speed measurements at 313°K show that the concentration dependence mainly retains

TABLE 5. Temperature Dependence of Calculated ΔG_m^0, ΔH_m^0 and ΔS_m^0

T, K	c_c		ΔG_m^0,	ΔH_m^0,	ΔS_m^0,
	mole/m^3	mp $\times 10^3$	kJ/mole	kJ/mole	J/mole·deg
293	10,0	0,18	—21,0	—7,1	47,2
303	11,0	0,20	—21,4	—7,5	45,6
313	12,0	0,22	—21,8	—8,0	44,0
323	13,0	0,24	—22,2	—8,8	41,4
333	15,0	0,28	—22,6	—9,2	40,2

the features found at 293°K, but the dependence is much weaker at 313°K. All the same, the width of the concentration region showing deviation from linearity is about the same.

OBS alters the molecular structure of the water, and one gets hydrophobic interactions arising from the amphiphilic structure. At certain OBS concentrations (the CMC), the correlation between the solute particles due to the hydrophobic interaction leads to the formation of a new unit: aggregates of OBS molecules, which are surrounded by water of hydration. This affects many macroscopic parameters, which can be used in judging the changes, e.g., the free energy ΔG_m^0, the enthalpy ΔH_m^0, and the entropy ΔS_m^0, whose changes can be determined from the temperature dependence of the CMC via

$$\Delta G_m^0 = RT \ln C_c, \quad \Delta H_m^0 = -RT^2 \left(\frac{\partial \ln C_c}{\partial T}\right)_p, \quad \Delta S_m^0 = R \ln C_c + \Delta H_m^0/T. \tag{16}$$

Table 5 gives the values for these parameters in OBS micelle formation.

The enthalpy of micelle formation is negative and small in magnitude, while the entropy is positive, so the entropy effects are important. This id due [4, 5] to an increase in the conformational entropy of the hydrocarbon chains in the micelles by comparison with the individual molecules in the bulk. This is confirmed by the positive volume effect (Table 1) when OBS molecules enter the micella state, where the thermal effect is slight.

The data indicate that the micelle formation occurs in an avalanche fashion in a narrow concentration range and produces an open microheterogeneous phase. The changes in entropy and partial molar volume are positive. Also, ΔV_m^0 is about 1.5 times larger for OBS solutions than ΔV_m^0 for SA having linear hydrophogic parts, which is evidently related to the benzene ring structure.

These studies show that the dependence of ρ, η, and u on OBS concentration far from the CMC is linear, with a link in the micelle-formation region; this linearity before and after the CMC indicates that the behavior is close to that for an ideal solution. The dependence on C for ρ, η, and u reflects the processes in the SA + water system, including the phase transition on micelle formation, while the speed of sound and the adiabatic compressibility are the parameters most sensitive to the structure changes.

NOTATION

a, b, coefficients in the linear density equation; K, m, the same for viscosity; ρ_0, ρ_c, density of water or solution at critical micelle formation concentration; M, molecular mass; v_1^0, $\bar{v}_2$, specific volumes of water and second component; R, universal gas constant; T, thermodynamic temperature.

LITERATURE CITED

1. A. A. Vedenov and E. B. Levchenko, "Supermolecular liquid-crystal structures in solutions of amphiphilic molecules," Usp. Fiz. Nauk, 141, No. 1, 3-53 (1983).
2. Mittel (ed.), Micelle Formation, Solubilization, and Microemulsions [Russian translation], Mir, Moscow (1980).
3. A. Voleišis and E. Jaronis, "An acoustic digital interferometer for examining the dispersion of the speed of ultrasound in liquids in the frequency range 0.25-1250 MHz," Nauch. Tr. VUZ Lit. SSR, Ul'trazvuk, No. 5, 11-28 (1973).
4. E. A. Arípov, M. A. Orel, and S. N. Aminov, Hydrophobic Interactions in Binary Solutions of Surfactants, Academician K. S. Akhmedov (ed.) [in Russian], Fan, Tashkent (1980).

5. A. A. Saidov, L. V. Pal'chikova, and I. I. Shinder, "Thermodynamics and molecular structure of the micelles in aqueous solutions of sodium p-n-octylbenzenesulfonate," Izv. Akad. Nauk Uz. SSR, Ser. Fiz.-Mat. Nauk, No. 6, 58-59 (1983).

EFFECTS OF HEAT TREATMENT ON THE PHONON THERMAL CONDUCTIVITY COMPONENT FOR KHROVANGAL ALLOY

V. V. Kukhar' and L. Yu. Rubashkina

UDC 536.212.2

A study has been made of the effects of alloying elements in Khrovangal nickel alloy on the phonon component of the thermal conductivity in heat-treated specimens.

A promising method of reducing the overall thermal conductivity of a nickel-base alloy is [1] appropriate heat treatment. We have examined the effects of heat treatment (tempering and ageing) on the phonon component. We used khrovangal alloy, which is a standard material with thermal conductivity 9.1 W/m·K at 300°K.

We examined 18 alloys containing alloying elements at the following levels in mass %: Cr 5-15, V 5-12, Mo 4-5, W 0-4, Re 0-5, Ga 5-12, Ge 0-3 [2]. From each alloy we made three specimens of diameter 15 mm and height 10 mm and one rod of length 100 mm and of the same diameter. The alloys were quenched from 1373°K and were then aged at 823°K for 5 h.

The thermal conductivities were measured with an ITÉM-1M apparatus, while the resistivity of the rods was measured by a potentiometric method.

The measured resistivities were used to calculate the electron component of the thermal conductivity λ_e from the Wiedmann-Franz law. The phonon component λ_p was derived by subtracting the electron component from the total conductivity λ. For nine alloys, λ_p was increased after ageing, while eight it was reduced, and in one λ_p remained virtually at the same level. We determined the change in λ_p due to aging $\Delta\lambda_p = \lambda_{pt} - \lambda_{pht}$ for all the alloys. The values were used to find the parameters in the linear dependence of $\Delta\lambda_p$ on alloying-element content. A computer was used to perform the regression and variance analyses [3]. The equation takes the form

$$\Delta\lambda_p = -11.78 + 2,3\,(\%\ \mathrm{Mo}) + 1.57\,(\%\ \mathrm{W}) - 1.24\,(\%\ \mathrm{Re}).$$

Therefore, rhenium increases λ_p after aging, while molybdenum and tungsten reduce it.

In a nickel alloy, aging after tempering or cold deformation leads to ordering of a special kind. The corresponding structural state is known by a special term: the K state and is characterized by elevated resistivity, lattice compression, and increased elastic modulus [4]. The latter indicates that the atomic binding forces are increased.

There is at present no theory relating the thermal conductivity of these alloys to solid-solution structure. In [5], there is a detailed consideration of λ_p for low alloys. The changes are dependent in the main on the ratio of the atomic radii for the matrix and minor component, as well as on the atomic masses, concentration, and stress factor. If we assume that these factors also influence λ_p for high alloys, then tungsten and rhenium should have approximately identical effects on λ_p (with allowance for concentration) because they have very similar masses and atomic radii (183.85 and 186.2 as masses and 1.549 Å and 1.520 Å as radii correspondingly), so they should produce identical changes in λ_p in the K state, where there is lattice compression. However, these elements have opposite effects on λ_p after aging. One can explain this only by incorporating the changes in the binding forces and the lattice distortion.

Mendeleev All-Union Metrological Research Institute, Leningrad. Translated from Inzhenerno-Fizicheskii Zhurnal, Vol. 50, No. 1, pp. 84-86, January, 1986. Original article submitted January 22, 1985.

0022-0841/86/5001-0069$12.50